Journal of Hazardous Materials 169 (2009) 419–427

Contents lists available at ScienceDirect

Journal of Hazardous Materials

journal homepage: www.elsevier.com/locate/jhazmat

Kinetics of adsorption of 2-chloroethylethylsulphide on Al_2O_3 nanoparticles with and without impregnants

Amit Saxena[1], Avanish Kumar Srivastava, Abha Sharma, Beer Singh*

P D Division, Defence R & D Establishment, Jhansi Road, Gwalior 474002, MP, India

ARTICLE INFO

Article history:
Received 26 November 2008
Received in revised form 24 March 2009
Accepted 24 March 2009
Available online 31 March 2009

Keywords:
Metal oxide nanoparticles
Impregnation
Adsorption kinetics
Degradation
2-Chloroethylethylsulphide (2-CEES)

ABSTRACT

Alumina nanoparticles in the size range of 2–30 nm and surface area 375 m^2/g were synthesized using aerogel route and then characterized using N_2–BET, SEM, TEM, XRD, FTIR and TGA techniques. Thereafter, these were impregnated with reactive chemicals and tested for their potential by conducting studies on kinetics of adsorption of 2-chloroethylethylsulphide (2-CEES) under static conditions. Kinetics was studied using linear driving force and Fickian diffusion model. The kinetics parameters such as equilibration constant, equilibration capacity, diffusional exponent and adsorbate–adsorbent interaction constant were also determined. AP-Al_2O_3 with 10% impregnation of MoVPA (V_3) and NaOH showed the maximum (574 mg/g) and minimum (88 mg/g) uptake of 2-CEES among impregnated systems respectively. All impregnated systems except NaOH impregnation showed the values of diffusional exponent to be <0.5, indicated the diffusion mechanism to be Fickian, whereas AP-Al_2O_3 with and without NaOH impregnation showed the diffusional mechanism to be anomalous. Hydrolysis and dehydrohalogenation reactions (identified using GC/MS technique) were found to be the route of degradation of 2-CEES.

1. Introduction

In recent years, the scientific community has shown increasing concern to find out the safe and effective ways to detoxify chemical warfare (CW) agents without endangering the human life or the environment. One of the important ways to achieve protection against these agents is to utilize suitable material, which can perform the function of both physisorption followed by chemisorption, i.e., initially the adsorbate molecules are physically adsorbed then they follow dissociative chemisorption to such an extent that the chemical integrity of the adsorbate molecule is completely destroyed [1,2].

Nanoparticles of metal oxides have received enormous interest in recent years because of their unique physical and chemical properties [3]. These high surface area materials have been synthesized via soft chemistry by sol–gel process [3], which is the most common and widely used "bottom-up" wet chemical method. First, Utamapanya et al. [4] in 1991 described the modified hypercritical drying process for the preparation of inorganic metal oxide nanoparticles by sol–gel process utilizing aerogel route. Fig. 1 provides a schematic with brief detail of the synthetic procedure in general. Remarkable contributions have been made by Klabunde and coworkers [5–7] for the preparation, characterization and application of nanosize metal oxide particles alone and in association with other oxides. Metal oxide particles alone show promising results against CW agents, but their efficiency can further be increased by loading/impregnating them with those reactive compounds, which have already been proven to be active against toxic agents [8–11], however, the possibility of new compounds for impregnation also exists. The use of polyoxometalates (POMs) for impregnation of nanosize metal oxides can be explored with confidence as these have already been proven to be useful for the degradation of toxicants [9–12].

Contaminated air can be made breathable by allowing it to come in contact with nanoparticles based systems under dynamic (flow of gas) or static (no flow of gas) conditions. Under static conditions kinetics of adsorption and diffusion of adsorbate over adsorbent have widely been investigated [8,13,14]. Several researchers [8,13] have used various models, such as Fickian [15], linear driving force (LDF) [16], a combined barrier resistance/Fickian diffusion and Langmuir type second order kinetics [17] to describe the adsorption kinetics in porous materials and carbon molecular sieves [18]. Saxena et al. [8] studied the kinetics of adsorption of dimethylmethylphosphonate in gas phase on carbon systems under static conditions and determined various kinetics parameters such as equilibration time (t), equilibration capacity (M_t), rate constant (k), diffusional exponent (n) and constant (K).

The analysis of reaction/degradation products is equally important as that of kinetics study. In order to find out reaction products these either have to be investigated directly using MAS–NMR

* Corresponding author. Fax: +91 751 2341148.
E-mail addresses: amsa888@rediffmail.com (A. Saxena), beerbs5@rediffmail.com (B. Singh).
[1] Fax: +91 751 2341148.

0304-3894/$ – see front matter.
doi:10.1016/j.jhazmat.2009.03.112

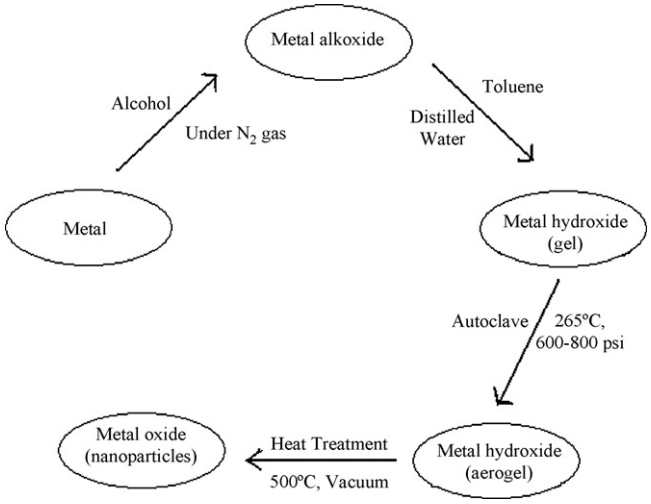

Fig. 1. General schematic for the synthesis of metal oxide nanoparticles.

technique [1,2] or by extracting them in organic solvent and analyzing through GC–MS [8]. The literature indicates that nanocrystals of metal oxides can degrade CW agents by variety of reactions, such as oxidation, hydrolysis, elimination and dealkylation [1,2,19].

It is always recommended to study the reactive systems with simulant of CW agents as simulants are less toxic and their use involves low risk than actual agents. Therefore, in the present study AP-Al_2O_3 nanoparticles with and without impregnants were synthesized and explored to adsorption kinetics of 2-CEES (a less toxic simulant of sulphur mustard). The objective of the present study was to identify the best impregnated AP-Al_2O_3 nanoparticles based system to remove 2-CCES and to understand mass transfer phenomena, mode of diffusion and adsorption characteristics of 2-CEES on AP-Al_2O_3 nanoparticles with and without impregnants. Suitable nanoparticles based systems can be used in decontamination devices, i.e., Handecon (an equipment under development to remove chemical warfare agents available as gases/vapors in the atmosphere) or filtration systems (by converting nanoparticles to granules by mechanical compression techniques) to remove chemical warfare agents.

2. Experimental

2.1. Synthesis of AP-Al_2O_3 nanoparticles

In order to synthesize AP-Al_2O_3 nanoparticles 10.0 g of aluminum powder cleaned with acetone immediately before the reaction was taken with 500 mL of methanol in 1000 mL round-bottom flask and connected to water condenser. The reactants were stirred at room temperature for 24 h under inert atmosphere of nitrogen gas. To this 425 mL of toluene was added and the solution was stirred for 30 min. A solution of stoichiometric amount, i.e., 20 mL (1.2 M) of triple distilled and deionized water in 230 mL of methanol and 675 mL of toluene was prepared. This solution was slowly added to the solution made in earlier with vigorous stirring in a 3.0 L round-bottom flask. The solution was covered with aluminum foil and stirred for 24 h. This resulted into slightly grey liquid like gel (Fig. 2a).

600 mL of thus produced aluminum hydroxide gel was transferred to 1000 mL capacity parr autoclave. The gel was first flushed with nitrogen, and the reaction was carried out under nitrogen, with an initial pressure of 100 psi. The reactor was slowly heated from room temperature to 265 °C at the rate of 1 °C/min. The reactor was maintained at 265 °C for 10 min and the system was quickly vented to the atmosphere for over a 1 min period, the furnace taken off and the aluminum hydroxide flushed with nitrogen for 15 min to remove the remaining solvent vapors. This produced fluffy light grey powder of AP-$Al(OH)_3$ (Fig. 2b).

20 g of thus produced nano-aluminum hydroxide powder was placed in 500 mL capacity thermal reactor. This was evacuated for 30 min at room temperature. Later, it was slowly heated for 6 h from room temperature to 500 °C under dynamic vacuum of 10^{-2} Torr and kept under this condition for 10 h. This resulted into the fine light grey powdery AP-Al_2O_3, which was due to the conversion of residual organic groups (–OCH_3) on AP-$Al(OH)_3$ to carbon during heat treatment of AP-$Al(OH)_3$ to AP-Al_2O_3 at 500 °C. Finally, the material was cooled to room temperature under vacuum, flushed with nitrogen and stored in air tight bottles till further use.

50–200 mg pellets with the density of 0.1–0.3 g/cm^3 were also prepared using manual pelletting machine by applying a pressure of 5.0–15 × 10^5 N/m^2. These pellets of different sizes (3–8 mm diameter and 5–15 mm height) were made and also broken down to granules of different sizes (Fig. 2c). Thus produced metal oxide gran-

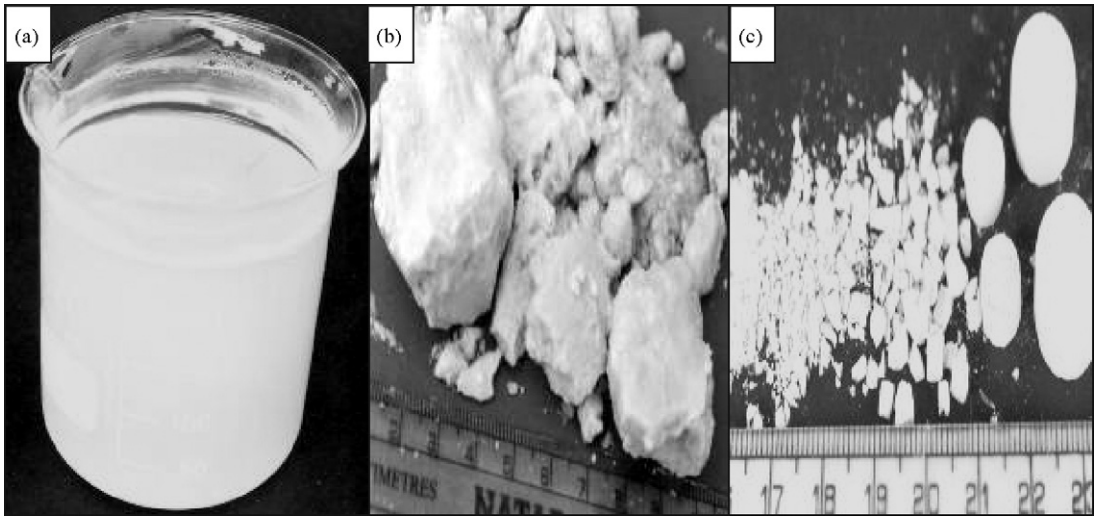

Fig. 2. (a) AP-$Al(OH)_3$ gel, (b) fluffy AP-$Al(OH)_3$ after supercritical drying and (c) powder, granules and pellets of prepared alumina nanoparticles based system.

Table 1
Surface area, pore size distributions, bulk density and moisture content of prepared nano-adsorbents.

Prepared adsorbent + impregnation percentage	Surface area (N_2 BET) (m^2/g)	Micropore volume (N_2 DR) (cm^3/g)	Cumulative desorption pore volume (N_2 BJH) (cm^3/g)	Pore maxima for micro- and mesopores (Å)		Bulk density (g/mL)	Moisture content (%)
				Micro	Meso		
AP-Al(OH)$_3$ + nil	563	0.21	1.12	8.2	34.5	0.05	1.9
AP-Al_2O_3 + nil	375	0.16	0.57	15.3	27.5	0.04	0.6
AP-Al_2O_3 + 10% NaOH	141	0.06	0.18	15.2	60.3	0.06	1.8
AP-Al_2O_3 + 10% MoVPA (V_3)	318	0.14	0.44	14.7	27.5	0.05	0.7
AP-Al_2O_3 + 10% PTA	312	0.14	0.41	14.6	27.8	0.05	3.1
AP-Al_2O_3 + 10% K_2OsO_4	300	0.13	0.41	13.9	59.4	0.05	1.9
CM-Al_2O_3 + nil	105	0.04	0.16	13.9	31.5	0.90	3.4

ules and pellets represent a new family of mesoporous inorganic material where pore structure can also be roughly controlled by compression technique. Thus produced material may have the possibilities of application in filtration/purification/decontamination systems.

2.2. Characterization of AP-Al_2O_3

2.2.1. Surface area and porosity

Surface area and pore size distribution of AP (aerogel produced nanoparticles) aluminum hydroxides/oxides and CM-Al_2O_3 (commercially available aluminum oxide particles) were determined using Autosorb-1-C from Quantachrome, USA. The samples were first outgassed under dynamic vacuum (10^{-2} Torr) for 8 h at 200 °C and then allowed to cool to room temperature. After that, the N_2 adsorption–desorption isotherms were obtained at liquid nitrogen temperature, i.e., 77 K. Surface area and micropore volume were determined using Brunauer–Emmet–Teller (BET) and Dubinin Radushkevich (DR) methods respectively. Cumulative desorption pore volume was determined using Barrett–Joyner–Halenda (BJH) method. Pore maxima for micropore (<2 nm) and mesopore (2–50 nm) were determined considering BJH and DFT (density functional theory) methods. The surface area, micropore volume, cumulative desorption pore volume and pore maxima for micropores and mesopores have been given in Table 1. Figs. 3 and 4 describe the nitrogen adsorption isotherms and pore size distributions of AP-Al(OH)$_3$, AP-Al_2O_3 and CM (commercial)-Al_2O_3.

2.2.2. Scanning electron microscopy/transmission electron microscopy and X-ray diffraction

For SEM characterization, the powder samples were first mounted on brass stubs using double sided adhesive tape and then gold coated for 8 min using ion sputter JEOL, JFC 1100 coating unit. The surface texture of metal oxide nanoparticles was observed using FEI ESEM Quanta 400. Figs. 5 and 6 represent the SEM images of AP-Al(OH)$_3$ and AP-Al_2O_3 respectively.

TEM studies were performed to find out the particle size of the synthesized aluminum hydroxide and oxide nanoparticles. For that 10 mg of AP-Al_2O_3 powder sample was mixed in 10 mL of pentane and sonicated for 2 h to achieve a better separation of the particles. A drop of supernatant of the solution was placed on the copper grid of 200 mesh size followed by carbon coating. TEM images were recorded using JEOL, JEM-1200 Ex. Figs. 7 and 8 represent the images of AP-Al(OH)$_3$ and AP-Al_2O_3 respectively.

For XRD studies the powder samples were heat treated under vacuum before placing onto the sample holder. The instrument used was Philips XRD PW 3020. Cu Kα radiation (λ = 0.154 nm) was the light source used with applied voltage of 40 kV and current of 40 mA. The 2θ angles ranged from 20 to 80° with a speed of 0.05°/s. The crystallite size was then calculated from the XRD spectra using Scherrer equation. Fig. 9 shows the XRD pattern of AP-Al(OH)$_3$ and AP-Al_2O_3.

2.2.3. Fourier transform infra-red spectroscopy and thermogravimetric analysis

Fourier transform infra-red study of AP-Al_2O_3 was performed to find out the complete solvent removal after heat treatment. For

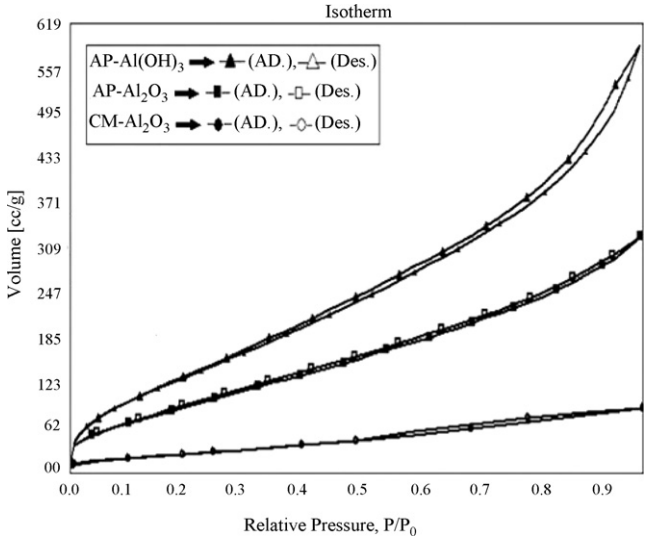

Fig. 3. Adsorption isotherms of AP-Al(OH)$_3$, AP-Al_2O_3 and CM-Al_2O_3.

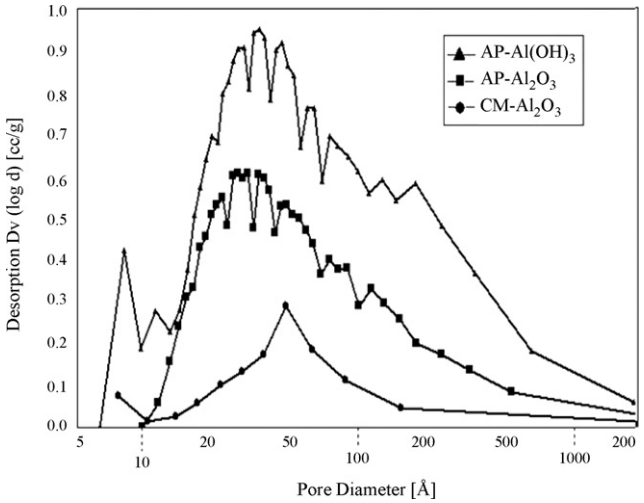

Fig. 4. BJH pore size distributions of AP-Al(OH)$_3$, AP-Al_2O_3 and CM-Al_2O_3.

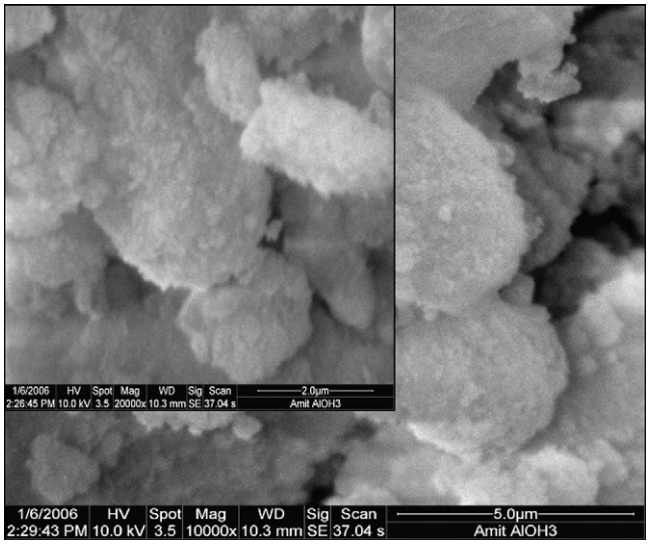

Fig. 5. SEM of AP-Al(OH)$_3$.

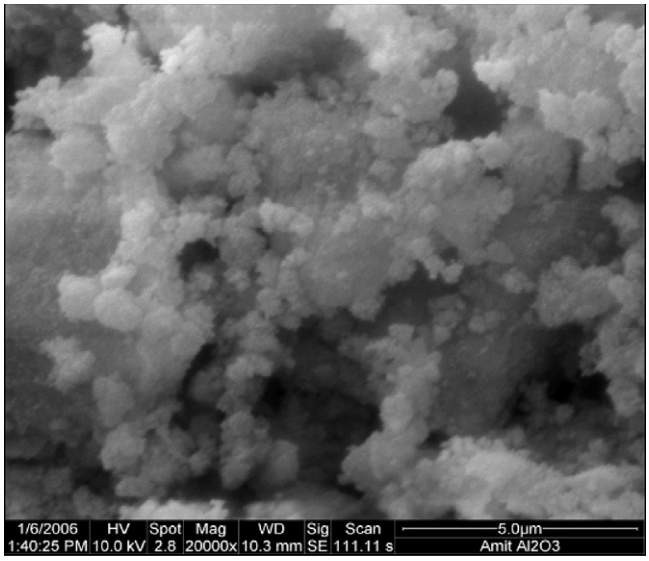

Fig. 6. SEM of AP-Al_2O_3.

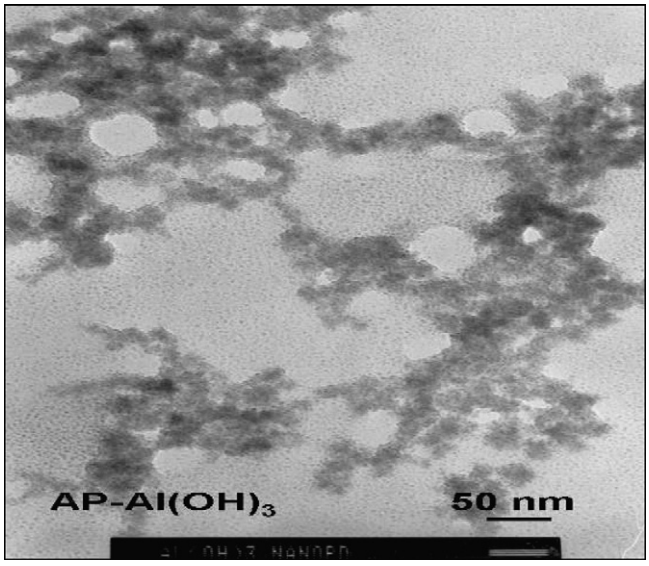

Fig. 7. TEM of AP-Al(OH)$_3$.

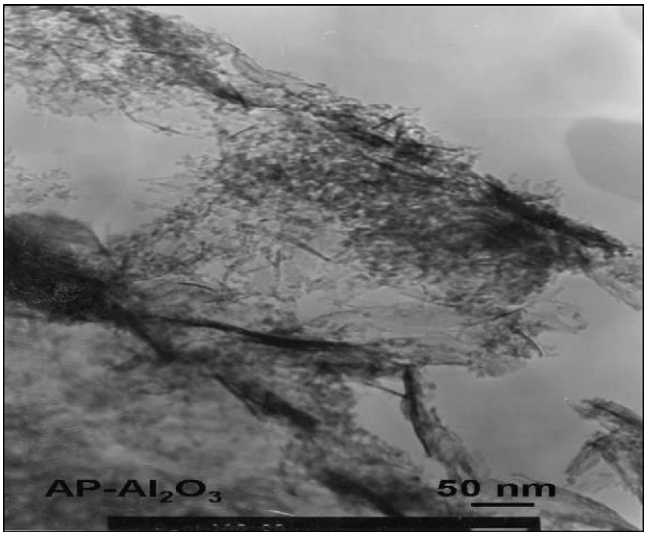

Fig. 8. TEM of AP-Al_2O_3.

that a few of the particles of powder nanosize alumina was mixed with 200 mg of potassium bromide, ground to make pellets, dried and finally recorded the IR spectra (Fig. 10).

TGA was used to study the conversion of nano-metal hydroxides to nano-metal oxides and make a comparison with commercial metal oxides. Thermograms for materials were recorded from 30 to 800 °C in air using thermogravimetric analyzer, TGA-2950 from TA Instruments, USA. The initial sample weight was always 10 mg and the heating rate was 20 °C/min. Fig. 11 shows the TGA profile.

2.2.4. Bulk density and moisture content

The bulk density of synthesized and commercial materials were measured by weighing a known volume (20 mL) of material and expressed in g/mL. The moisture content of the material was determined by heating a known amount (1 g) of sample in oven at 120 °C for 6 h, cooling in desiccators for 1 h and finally weighing. The weight loss in sample per 100 g was taken as moisture content of the material. The bulk density and moisture content results have been described in Table 1.

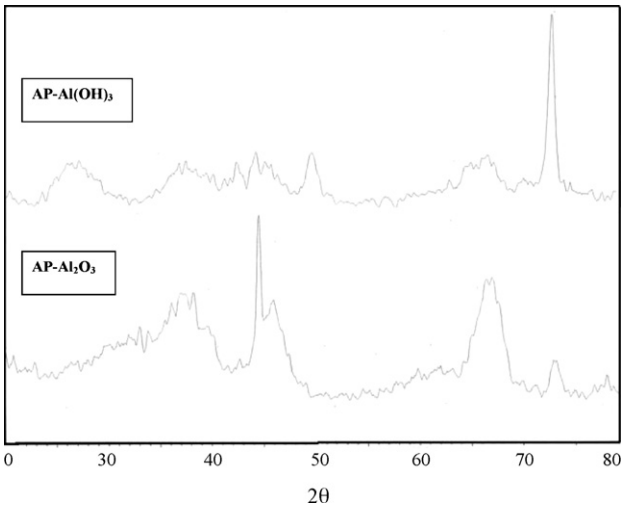

Fig. 9. XRD pattern of AP-Al(OH)$_3$ and AP-Al_2O_3.

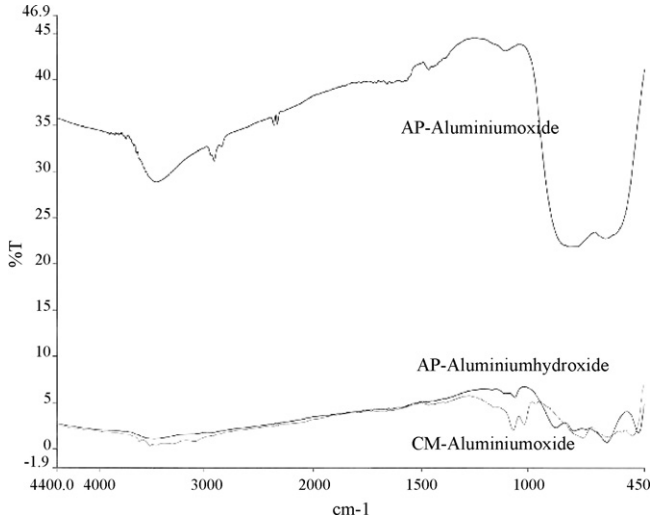

Fig. 10. FTIR of AP-Al(OH)$_3$, AP-Al_2O_3 and CM-Al_2O_3.

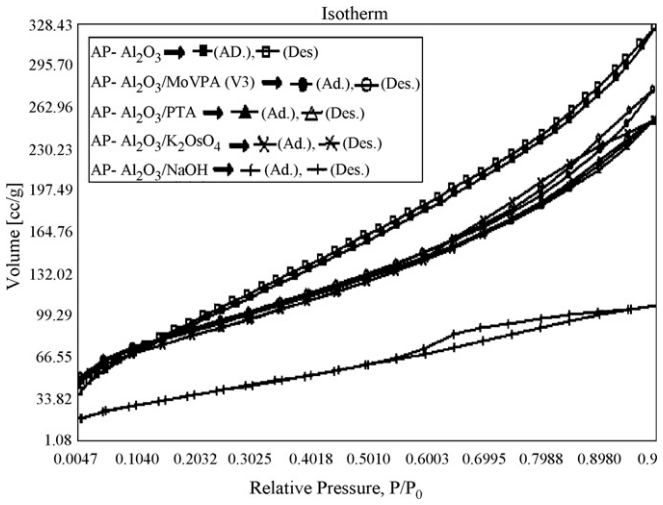

Fig. 12. Adsorption isotherms of AP-Al_2O_3 with and without impregnants.

2.3. Loading of impregnants on alumina nanoparticles

In order to prepare impregnated alumina nanoparticles AP-Al_2O_3 was separately impregnated (10%, w/w) with 9-molybdo-3-vanadophosphoric acid [{MoVPA (V_3)}:$H_6[PMo_9V_3O_{40}]\cdot 34H_2O$], dodeca tungstophosphoric acid {(PTA): $H_3PW_{12}O_{40}\cdot xH_2O$}, NaOH and K_2OsO_4. For impregnation the solution of impregnants in water (corresponding to incipient volume of AP-Al_2O_3 nanoparticles, i.e., 400 μL/100 mg of AP-Al_2O_3) was prepared and the technique used for this was incipient wetness technique [8]. This technique allows the impregnant solution to just wet the adsorbent and allows the complete adsorption of impregnant on solid adsorbent. Thereafter, impregnated systems were dried at 110 °C for 4 h, cooled in desiccators and finally stored in airtight bottles till further use. These were also characterized (Table 1 and Figs. 12 and 13) for surface area, pore size distributions, bulk density and moisture content.

2.4. Static adsorption studies

In order to carry out the adsorption of 2-CEES under static conditions, 50 mg each of AP-Al_2O_3 with and without impregnants was taken separately in gooch crucibles and placed on perforated disc in a closed glass chamber in which 5.0 mL of 2-CEES was placed at the bottom of chamber. To maintain constant temperature, the glass chamber along with weighing balance was housed in an oven kept at 33 ± 1 °C. Vapor pressure of 2-CEES in the glass chamber was measured and found to be 3.35 mm Hg at 33 °C. The kinetics of adsorption of 2-CEES was studied by monitoring the percentage of weight gain every hour. Since moisture free air was not used to monitor the kinetics of adsorption of 2-CEES, the possibility of co-adsorption of atmospheric moisture cannot be ruled out. However, the co-adsorption of water will be insignificant and will not affect the adsorption of 2-CEES due to very little influence of humidity on adsorption of toxicants [20].

Of the above, the concentration of gas was considered to be constant at atmospheric pressure in the glass chamber. As the adsorption of toxicant by the nanoparticles based adsorbents starts it causes the depletion in vapor phase concentration of toxicant in the glass chamber. The depletion in concentration is compensated by liquid phase toxicant, which was placed at the bottom of the glass chamber. Therefore, the concentration of toxicant vapor in the glass chamber remains constant and it ensures a continuous supply of toxicant to the adsorbent. Figs. 14, 15 and 16 represent the kinetics of uptake, diffusion and adsorption of 2-CEES on prepared systems respectively. Table 2 represents the kinetics parameters.

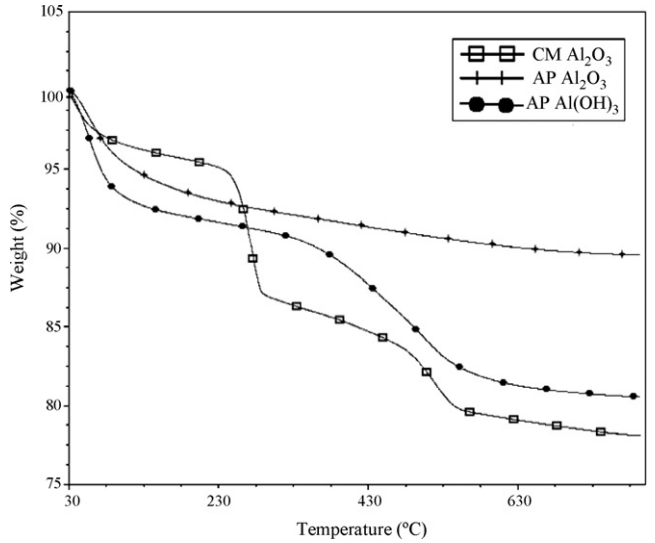

Fig. 11. Thermograms of AP-Al(OH)$_3$, AP-Al_2O_3 and CM-Al_2O_3.

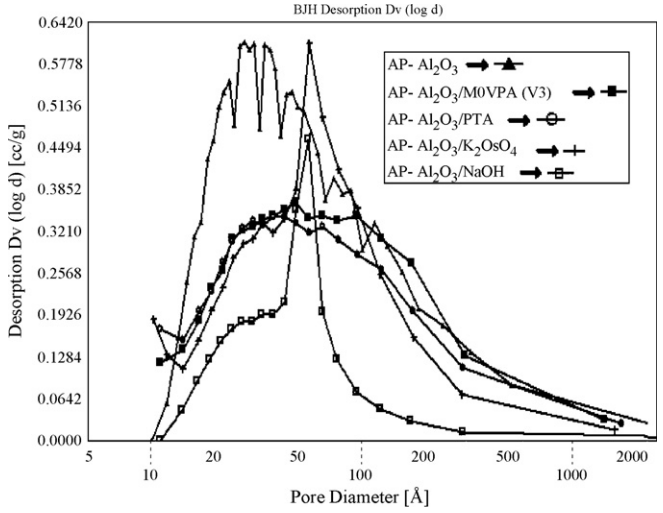

Fig. 13. BJH pore size distributions of AP-Al_2O_3 with and without impregnants.

Table 2
Kinetics parameters for the adsorption of 2-CEES on prepared nano-adsorbents.

Prepared adsorbent + impregnation percentage	Equilibration time (h)	Equilibration capacity (mg/g)	Diffusional exponent (n)	Constant (K) (h^{-1})	Rate constant (k) (h^{-1}) $\times 10^{-2}$
AP-Al_2O_3 + nil	170	1694	0.74	0.11	1.8
AP-Al_2O_3 + 10% NaOH	28	88	0.54	0.45	7.6
AP-Al_2O_3 + 10% MoVPA (V_3)	45	574	0.43	0.39	6.9
AP-Al_2O_3 + 10% PTA	46	520	0.42	0.48	10.0
AP-Al_2O_3 + 10% K_2OsO_4	31	326	0.13	0.77	14.5

2.5. Identification of reaction products

In order to investigate the reaction products 10 mg of 2-CEES exposed alumina nanoparticles were extracted with 2.0 mL of acetonitrile for 2 h in a well stoppered test tube. The extracts were centrifuged, transferred to another tube and purged with nitrogen gas to concentrate the extracted reaction products and finally subjected to product identification using GC/MS (gas chromatograph coupled with mass spectrometer) instrumental techniques. GC/MS (6890N GC coupled with 5973 inert MS detector) of Agilent Technologies, USA was used for characterization of reaction products. It was equipped with HP-5 MS column of 30 m × 0.25 mm × 0.25 μm dimensions. Temperature programming [50 (2 min hold) to 280 °C (10 min hold) at 10 °C/min] with split injection technique (10:1) was used to perform the study. Injection port and GC/MS interface, MS source and quadrupole analyzer were kept at 280, 230 and 150 °C respectively. The mass spectra of reaction products were compared with the standard mass spectra from existing libraries (Wiley and NIST) of GC/MS instrument.

3. Results and discussion

3.1. Characterization of alumina nanoparticles based adsorbents

Nitrogen adsorption–desorption isotherms and BJH pore size distributions of AP-Al$(OH)_3$, AP-Al_2O_3 and CM-Al_2O_3 have been represented in Figs. 3 and 4. AP-Al$(OH)_3$ showed highest uptake of nitrogen and exhibited broad hysteresis loop, which are characteristic of adsorption possessing a high portion of mesopores. Fig. 3 clearly indicated that AP-Al$(OH)_3$, AP-Al_2O_3 and CM-Al_2O_3 have the similar type of pore size distributions with mesopore maxima at 34.5, 27.5 and 31.5 Å (Table 1) respectively. Apart from mesoporous characteristic AP-Al$(OH)_3$ and AP-Al_2O_3 were also found to be having micropores with DR micropore volume of 0.21 and 0.16 cm^3/g respectively. The surface area of AP-Al$(OH)_3$ was found to be 563 m^2/g. On heat treatment of AP-Al$(OH)_3$ to AP-Al_2O_3 at 500 °C the surface area decreased to 375 m^2/g. Micropore and cumulative desorption pore volume were also found to be decreased. Moreover, this decrease was due to the dehydration process, which causes severe sintering and damage to the pore structure [4]. Surface area of AP-Al_2O_3 was found to be 3.6 times of that of the material commercially available (CM-Al_2O_3).

Figs. 5–8 show the SEM and TEM images of AP-Al$(OH)_3$ and AP-Al_2O_3. SEM images of AP-Al$(OH)_3$ (Fig. 5) and AP-Al_2O_3 (Fig. 6) indicated the material to be having a multitude of thin strands to give fluffy and porous weblike structure with wide particle size distributions. TEM images of AP-Al$(OH)_3$ (Fig. 7) and AP-Al_2O_3 (Fig. 8) indicated these materials consist of weblike structure [5] with the particle diameter in the range of 4–30 (maximum particles of 20 nm diameter) and 3–14 (maximum particles of 10 nm diameter) nm respectively. Imaging at different scales was performed to estimate correctly the proportion of small particles (2–10 nm) and embedded in agglomerates (10–100 nm). Furthermore, the particles overlapping in agglomerates lead to quite noisy images making the determination of proportion and size of the smallest particle population a very difficult task. Synthesized nanoparticles showed the decrease in particle diameter on conversion from hydroxides to oxides. Smallest particles were of 3 nm diameter, however, three to four crystallites aggregate into ~10 nm particles, and these particles weakly agglomerate into a mass with large pores, where the pores are actually the space between the particles (as opposed to holes and channels in the particles themselves). XRD spectra of AP-Al$(OH)_3$ and AP-Al_2O_3 indicated an amorphous pattern due to peak broadening with the particle diameter in the range of 2–17 nm (Fig. 9). Moreover, the study of synthesized nanoparticles using SEM/TEM and XRD has clearly indicated them to be nanoparticles of diameter in the range of 2–30 nm.

Fig. 10 represents the IR spectra of prepared and commercially available samples. IR spectrum of AP-Al_2O_3 indicated two absorption peaks at 3600 cm^{-1} corresponding to associated OH groups and at 3700 cm^{-1} corresponding to isolated surface OH groups [5]. Less intensity of peaks at 1080 and 2800–2950 cm^{-1} with AP-Al$(OH)_3$ and AP-Al_2O_3 clearly indicated the removal of methoxide groups by heat treatment at 500 °C for the conversion of AP-Al$(OH)_3$ to AP-Al_2O_3. Fig. 11 shows the TGA profile of AP-Al$(OH)_3$, which indicated the weight loss of 8.2% between 30 and 170 °C (due to the desorption of physisorbed water and organic moieties). Desorption of chemisorbed water and organic groups occurred between 170 and 310 °C and it produced a weight loss of only 1.2%. The pronounced weight loss of 10.2% observed between 310 and 600 °C was produced by dehydroxylation of AP-Al$(OH)_3$ to AP-Al_2O_3 [5]. The total loss was 20.5%, whereas the conversion of Al$(OH)_3$ to Al_2O_3 should yield a weight loss of 35 and conversion to AlOOH would be 23% [5]. Therefore, lesser value of weight loss, i.e., 20.5% indicated that AP-Al$(OH)_3$ also contain some part of AP-Al_2O_3, which remains as such on heat treatment and does not result decrease in weight. AP-Al_2O_3 indicated the weight loss of ~6.0% up to 110 °C due to adsorbed water.

Subsequently, the material was also characterized for bulk density, which was found to be much less than the material available commercially. This was because of their fluffy and powdery nature. All prepared alumina nanoparticles based systems indicated bulk densities within 0.04–0.06 g/mL (Table 1). Bulk density of AP-Al_2O_3 was found to be 0.04 g/mL, which is 1/22 of that of commercially available CM-Al_2O_3 (0.90 g/mL). Moisture content of synthesized and commercial particles was found to be <3.1% (Table 1).

Figs. 12 and 13 represent the nitrogen adsorption–desorption isotherms and BJH pore size distributions of AP-Al_2O_3 with and without impregnation. Table 1 represents the surface area, pore size distributions, bulk density and moisture content of all impregnated AP-aluminum oxides. AP-Al_2O_3 impregnated with MoVPA (V_3) and NaOH [10% (w/w)] showed the highest and lowest uptake of nitrogen among impregnated nanoparticles respectively (Fig. 12). AP-Al_2O_3 when was impregnated with MoVPA (V_3) [10% (w/w)], surface area decreased from 375 to 318 m^2/g. This decrease was due to impregnants, which during impregnation travel through the macropores and gets deposited in the mesopores or the pore opening of micropores to cause the blocking of the meso/micropores [8–10]. Decrease in surface area after impregnation was found with all samples (Table 1). AP-Al_2O_3 with NaOH impregnation (10%, w/w) showed maximum reduction in surface area, i.e., from 375 to 141 m^2/g (~1/3 of unimpregnated nanoparticles). This was due

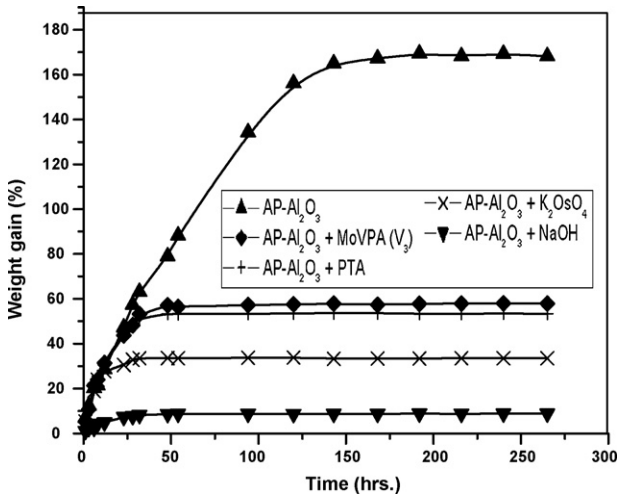

Fig. 14. Kinetics of uptake of 2-CEES on prepared alumina nanoparticles based adsorbents.

to the impregnation of NaOH, which results similar to lump formation and give rise to the reduction in volume of the system, i.e., decrease in surface area and pore volume. Pore maxima for micropores of AP-Al_2O_3 with impregnation were found to be ~14 Å. The mesopore maxima for NaOH and K_2OsO_4 impregnated AP-Al_2O_3 was found to be to be ~60 Å, which was higher than other systems (Table 1 and Fig. 13). Aerogel prepared and commercial aluminum oxides indicated the increase in bulk densities after impregnation due to the reason that impregnants sit in the pores, the volume of the material remains same, whereas weight increases, hence density increases. Surface area and cumulative desorption pore volume of pellets/granules of AP-Al_2O_3 were found to be within the range of 328–368 m^2/g and 0.60–0.64 cm^3/g respectively. These values are lesser than the values of corresponding metal oxide nanoparticles. This decrease is because of the compression, which collapses the pores within/between nano-aggregates of nanoparticles [21]. This has indicated that the pore structure and surface area of nanoparticles based adsorbents can roughly be controlled by compression technique.

3.2. Kinetics of adsorption of 2-CEES

To illustrate the kinetics of adsorption of 2-CEES, percentage weight gain of adsorbate was plotted versus time (t) and represented graphically in Fig. 14. Fig. 14 shows the similar shape of 2-CEES adsorption uptake curves and different adsorption rates for studied nanoAP-Al_2O_3 based adsorbent systems. Fig. 14 was used to compute the equilibration time (the time at which the adsorption ceases, i.e., no change in weight gain with respect to time) and equilibration capacity (amount of adsorbate in mg/g of adsorbent at equilibration time), and the values have been tabulated in Table 2. At initial stage the rate of adsorption was fast, which gradually slowed down to a steady state at later intervals of time. Highest value of equilibration time (170 h, Table 2) was found with unimpregnated AP-Al_2O_3 system, whereas with other systems the equilibrium reached within 50 min. AP-Al_2O_3 system also showed the highest equilibration capacity (1694 mg/g) among studied systems. This was slightly in agreement with the values of surface area, as higher the surface area higher will be the adsorption capacity. The values of equilibration capacity/surface area were found to be 4.5 and 1.8 for AP-Al_2O_3 and AP-Al_2O_3 + MoVPA (V_3) systems respectively. High value with AP-Al_2O_3 system indicated the possibilities of condensation of 2-CEES.

When AP-Al_2O_3 (surface area = 375 m^2/g) was impregnated with impregnants (e.g. NaOH), it showed a decrease of ~62% in surface area, whereas the adsorption capacity for 2-CEES adsorption decreased by ~95%. Decrease in adsorption potential with impregnated systems was because of impregnants, which work as a barrier and resist the movement of adsorbate molecules [8–10]. Among impregnated systems AP-Al_2O_3 + MoVPA (V_3) and AP-Al_2O_3 + NaOH systems showed the highest (574 mg/g) and lowest (88 mg/g) values of equilibration capacity respectively. Lowest adsorption potential with AP-Al_2O_3 + NaOH system clearly indicated that it was due to the destructive reaction of NaOH with alumina nanoparticles. Moreover, the study (Table 2) indicated that polyoxometalate (MoVPA (V_3) or PTA) impregnated alumina nanoparticles favors the adsorption of 2-CEES, whereas sodium hydroxide impregnation to alumina nanoparticles is not supportive.

The study indicated that the transport of 2-CEES into nano-adsorbent systems is a complex process. It is quite evident from the fact that alumina nanoparticles contain wide pore size distribution, which makes the analysis of adsorption kinetics more complex. The adsorption process involves diffusion in slit shaped micropores with pore widths considerably smaller than the mean free path of the gas molecules at atmospheric pressure [18]. It is likely that processes such as molecular diffusion, Knudsen diffusion, surface diffusion, diffusion in micropores and the chemical interaction of 2-CEES with the functional groups of nanoparticles and the impregnants in it could all make contributions to the adsorption kinetics.

Modeling of kinetic process being difficult due to wide pore size distribution, the two simple approaches are to use either Ficks diffusion laws for homogeneous materials or to describe the process by Phenomenological model. Although, the particles under study are not homogeneous and spherical, if we assume surface concentration of gas to be constant and that diffusion is controlled by the concentration gradient through the granule then the kinetics of the diffusion can be expressed by the following empirical diffusion equation [18,22].

$$\frac{M_t}{M_e} = K\,t^n \tag{1}$$

where M_t = gas uptake at time t, M_e = gas uptake at equilibrium, K = constant, t = time and n = diffusional exponent.

A graph of log M_t/M_e against log t (Fig. 15) was found to be a straight line at shorter intervals of time and the plots deviated from linearity for all the systems at higher t values. This deviation can be ascribed to the wide pore size distribution of prepared systems (Fig. 13). The diffusional exponent (n) values were computed by using the slope of straight line in Fig. 15. AP-Al_2O_3 with and

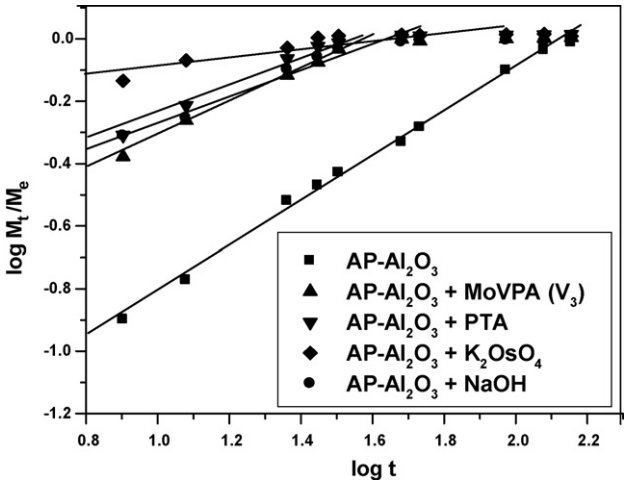

Fig. 15. Kinetics of diffusion of 2-CEES on prepared alumina nano-adsorbents.

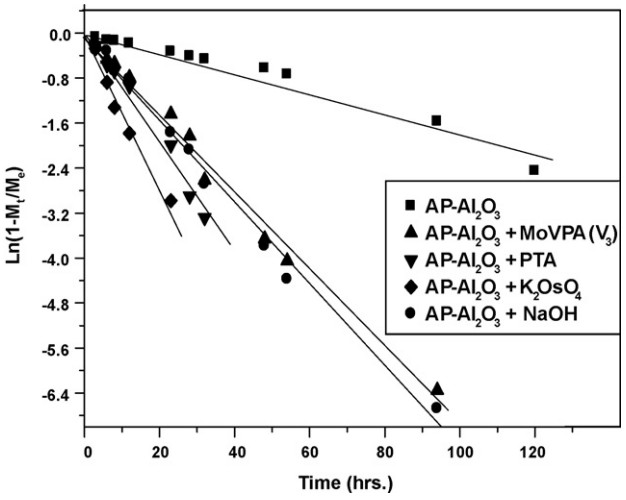

Fig. 16. Kinetics of adsorption of 2-CEES on prepared alumina nano-adsorbents.

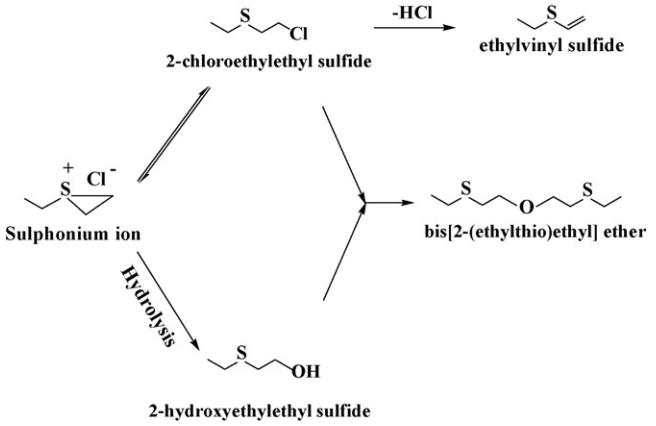

Scheme 1. Degradation products of 2-CEES on alumina nanoparticles based adsorbents.

without NaOH showed the diffusional exponent n being in between 0.5 and 1.0, it indicated the diffusion mechanism to be anomalous, whereas other system showed Fickian diffusion mechanism [15]. The value for constant K, adsorbate–adsorbent interaction coefficient was determined from the intercept of straight line on Y-axis. The K values were more or less the result of adsorption kinetics at lower t values. In present study the highest and lowest values of K (0.77 and 0.11 h^{-1}) were shown by AP-Al_2O_3 + K_2OsO_4 and AP-Al_2O_3 + nil systems respectively. Highest values of constant K with AP-Al_2O_3 + K_2OsO_4 system indicated the fastest initial adsorption kinetics (Fig. 14). AP-Al_2O_3 system with least value of K indicated the overall slowest adsorption kinetics with maximum adsorption potential (equilibration capacity). AP-Al_2O_3 + MoVPA (V_3) and AP-Al_2O_3 + PTA systems with nearer values of equilibration time capacity showed a small difference in K value, which may be within the experimental precision.

The gas uptake into nanoparticles may be considered as a pseudo-first order mass transfer between the gas phase and the adsorption sites [18,22]. The following phenomenological model, which is equivalent to a linear driving force mass transfer model, can represent the rate of uptake of toxicant.

$$\frac{M_t}{M_e} = 1 - e^{kt} \quad (2)$$

where k is rate constant.

Plots of ln $(1 - M_t/M_e)$ against time t (Fig. 16) result a straight line, which clearly indicated that the adsorption of 2-CEES on alumina nanoparticles with and without impregnants follows LDF mass transfer kinetic model. Pore size distribution being wide in the studied systems could not adversely affect the applicability of the LDF model at initial intervals of time; however, at longer intervals of time, the curves obtained by making use of the LDF model deviated from linearity, questioning its applicability. Nevertheless, the initial linear portions can be used to evaluate the adsorption parameters, which make the LDF model persuasive. Using LDF model the adsorption kinetics can be compared in terms of the rate constant (k), which indicates the rate of adsorption of 2-CEES as the system approaches to equilibrium. Rate constant, k can either be determined from the gradient of the kinetic plot as shown in Fig. 16 or by fitting the adsorption uptake curves to Eq. (2). Maximum and minimum values for rate constant k (Table 2) were found to be in similar order as that of K values. Lowest value of k (1.8×10^{-2} h^{-1}) with AP-Al_2O_3 + nil system was because of Fig. 16, which more or less represents the adsorption kinetics at lower t values. Higher equilibration time with this system also lowered the rate constant. AP-Al_2O_3 + MoVPA (V_3) system showed the lowest value of k (6.9×10^{-2} h^{-1}) among impregnated systems. Based on these results it can be inferred that AP-Al_2O_3 + MoVPA (V_3) system (with maximum adsorption potential among impregnated systems and considerable values of k/K) is the best system for the removal of 2-CEES from simulated contaminated zones (as 2-CEES vapors in closed glass chamber).

3.3. Identification of reaction products

Results indicated that on the surface of AP-Al_2O_3 with and without impregnants 2-CEES undergoes the hydrolysis reaction (Scheme 1) with the formation of intermediate sulphonium ion [23]. Sulphonium ion is formed due to the attack of sulfide on the β carbon atom of 2-CEES and is considered to be SN^1 reaction with anchimeric assistance. Sulphonium ion is highly unstable, because of which it could not be extracted and detected. Subsequently, the sulphonium ion undergoes hydrolysis with the water (as indicated in TGA pattern of AP-Al_2O_3 nanoparticles) available with nanoparticles under study (moisture content, Table 1) (no more water is added prior to the reaction) and results to 2-hydroxyethylethyl sulfide (2-HEES) as a reaction product. Dehydrohalogenation reaction was also found to be occurring to decontaminate 2-CEES to its corresponding vinyl product (ethylvinyl sulfide). Apart from that, bis[2-(ethylthio)ethyl] ether was also identified as a reaction product, which is formed either via the combination of two 2-HEES molecules with removal of one water molecule or the combination of 2-CEES and 2-HEES (one molecule each) with the removal of HCl. All studied systems showed the similar reaction products.

4. Conclusions

AP-Al_2O_3 nanoparticles were found to be mesoporous materials with little microporous characteristics. SEM/TEM and XRD analysis clearly indicated the material to be nanoparticles of diameter ranging from 2 to 30 nm. AP-Al_2O_3 + MoVPA (V_3) and AP-Al_2O_3 + NaOH systems showed the maximum and minimum equilibration capacities among impregnated systems respectively. For AP-Al_2O_3 + 10% NaOH and AP-Al_2O_3 + nil systems, diffusional exponent (n) values were found to be in between 0.5 and 1.0, indicating the diffusion mechanism to be anomalous, where as other systems indicated the values of n being <0.5; this depicted the diffusion mechanism to be Fickian. AP-Al_2O_3 + MoVPA (V_3) system showed the lowest value of K and k with maximum uptake (574 mg/g) of 2-CEES among impregnated systems. Alumina nanoparticles impregnated with MoVPA (V_3) degraded 2-CEES to 2-hydroxyethylethyl sulfide, ethylvinyl sulfide and bis[2-(ethylthio)ethyl] ether. Based on these results,

it can be inferred from that 9-Molybdo-3-vanadophosphoric acid (10%, w/w) impregnated AP-Al_2O_3 nanoparticles based novel reactive sorbents can promisingly be used in decontamination devices or filtration systems to toxicants available as gases/vapors in the atmosphere.

Acknowledgements

We thank Dr R. Vijayaraghavan, Director, DRDE, Gwalior for providing lab facilities to carry out and publish this work. We also thank Dr. M.V.S. Suryanarayana, Dr K. Ganesan, Dr R.P. Semwal and Dr P.K. Gutch for useful suggestions.

References

[1] G.W. Wagner, P.W. Bartram, O. Koper, K.J. Klabunde, Reactions of VX, GD, and HD with nanosize MgO, J. Phys. Chem. B. 103 (1999) 3225–3228.
[2] G.W. Wagner, L.R. Procell, R.J. O'Corner, S. Munavalli, C.L. Carnes, P.N. Kapoor, K.J. Klabunde, Reactions of VX, GB, GD, and HD with nanosize Al_2O_3—formation of aluminophosphonates, J. Am. Chem. Soc. 123 (2001) 1636–1644.
[3] K.J. Klabunde, Nanoscale Materials in Chemistry, John Wiley and Sons, New York, 2001.
[4] S. Utamapanya, K.J. Klabunde, J.R. Schlup, Nanoscale metal oxide particles/clusters as chemical reagents. Synthesis and properties of ultrahigh surface area magnesium hydroxide and magnesium oxide, Chem. Mater. 3 (1991) 175–181.
[5] C.L. Carnes, P.N. Kapoor, K.J. Klabunde, Synthesis, characterization, and adsorption studies of nanocrystalline aluminum oxide and a bimetallic nanocrystalline aluminum oxide/magnesium oxide, Chem. Mater. 14 (2002) 2922–2929.
[6] O. Koper, K.J. Klabunde, Reactive nanoparticles as destructive adsorbents for biological and chemical contamination, US Patent WO 01/78506 A1 (2001).
[7] K.J. Klabunde, J. Stark, O. Koper, C. Mohs, D.G. Park, S. Decker, Y. Jiang, I. Lagadic, D. Zhang, Nanocrystals as stoichiometric reagents with unique surface chemistry, J. Phys. Chem. 100 (1996) 12142–12153.
[8] A. Saxena, B. Singh, A. Sharma, V. Dubey, R.P. Semwal, M.V.S. Suryanarayana, V.K. Rao, K. Sekhar, Adsorption of dimethylmethylphosphonate on metal impregnated carbons under static conditions, J. Hazard. Mater. 134 (1–3) (2006) 104–111.
[9] A. Sharma, A. Saxena, B. Singh, M. Sharma, M.V.S. Suryanarayana, R.P. Semwal, K. Ganeshan, K. Sekhar, In situ degradation of sulphur mustard and its simulants on the surface of impregnated carbon systems, J. Hazard. Mater. 133 (1–3) (2006) 106–112.
[10] A. Sharma, A. Saxena, B. Singh, M.V.S. Suryanarayana, K. Ganesan, K. Sekhar, K.K. Dwivedi, Development and evaluation of modified whetlerite, an adsorbent material for in situ degradation of sulphur mustard, Carbon 44 (2006) 907–912.
[11] N. Okun, C.L. Hill, Materials for degrading contaminants, US Patent WO 03/094977 A2 (2003).
[12] M.L. Shih, W.D. Korte, J.R. Smith, L.L. Szafraniec, Reactions of sulfides with S-330, a potential decontaminant of sulphur mustard in formulations, J. Appl. Toxicol. 19 (1999) S83–S88.
[13] G.K. Prasad, B. Singh, A. Saxena, Kinetics of adsorption of sulfur mustard vapors on carbons under static conditions, AIChE J. 52 (2) (2006) 678–682.
[14] J. Crank, The Mathematics of Diffusion, Clerendon Press, Oxford, 1956.
[15] C.R. Reid, I.P.O. Koye, K.M. Thomas, Adsorption of gases on carbon molecular sieves used for air separation: spherical adsorptives as probes for kinetic selectivity, Langmuir 14 (9) (1998) 2415–2425.
[16] D.E. Ulberg, K.E. Gubbins, Selective adsorption of vapors on graphitic carbon, Mol. Phys. 84 (6) (1995) 1139–1153.
[17] K.F. Loughlin, M.M. Hassan, A.I. Fatehi, M. Zahur, Rate and equilibrium sorption parameters for nitrogen and methane on carbon molecular sieve, Gas Sep. Purif. 7 (4) (1993) 264–273.
[18] H.K. Chagger, F.E. Ndaji, M.L. Sykes, K.M. Thomas, Kinetics of adsorption and diffusional characteristics of carbon molecular sieves, Carbon 33 (10) (1995) 1405–1411.
[19] G.W. Wagner, O.B. Koper, E. Lucas, S. Decker, K.J. Klabunde, Reactions of VX, GD, and HD with nanosize CaO: autocatalytic dehydrohalogenation of HD, J. Phys. Chem. B 104 (2000) 5118–5123.
[20] O. Busmundrud, Vapour breakthrough in activated carbon beds, Carbon 31 (2) (1993) 279–286.
[21] R. Richards, W. Li, S. Decker, C. Davidson, O. Koper, V. Zaikovski, A. Volodin, T. Rieker, K.J. Klabunde, Consolidation of metal oxide nanocrystals. Reactive pellets with controllable pore structure that represent a new family of porous, inorganic materials, J. Am. Chem. Soc. 122 (20) (2000) 4921–4925.
[22] N.J. Foley, K.M. Thomas, P.L. Forshaw, D. Stanton, P.R. Norman, Kinetics of water vapour adsorption on active carbon, Langmuir 13 (7) (1997) 2083–2084.
[23] P.D. Bartlett, C.G. Swain, Kinetics of hydrolysis and displacement reactions of b,b'-dichlorodiethyl sulfide (mustard gas) and of b-chloro-b-hydroxydiethyl sulfide (mustard chlorohydrin), J. Am. Chem. Soc. 71 (1949) 1406–1415.